Design of Thermal Interface Material With High Thermal Conductivity and Measurement Apparatus

Jong-Jin Park
e-mail: parkjj@u.washington.edu

Minoru Taya
e-mail: tayam@u.washington.edu

Center for Intelligent Materials and Systems,
Department of Mechanical Engineering,
University of Washington,
Box 352600,
Seattle, WA 98195-2600

A thermal interface material (TIM) is a crucial material for transferring heat from a die to a heatsink. We developed a new TIM composed of carbon nanotubes, silicon thermal grease, and chloroform. The thermal impedance of the TIM was measured using a new device based on thermometer principles to measure thermal impedance and resistance. This device consists of an alumina substrate, titanium tungsten (TiW) layers, gold layers, and thin alumina layers. Then the measured thermal conductivity of the TIM was compared with predictions made by the thermal resistor network model, and the experimental results were found to be consistent with the predictions made by the model.
[DOI: 10.1115/1.2159008]

Keywords: resistor network model, thermal impedance, thermal interface material, thermal resistance, thermometer, thin film

1 Introduction

Thermal management is a key task for an electronic packaging engineer working on high power microprocessors and pumped laser diodes. There are two technical issues associated with thermal management, (i) design of a TIM that transports high heat flux emitting from a microprocessor or pumped laser diode effectively and promptly, and (ii) accurate measurement of the thermal properties of the TIM. We shall review below the previous works relevant to this technology.

Solbrekken developed a TIM tester to screen grease, phase change material, and elastomer type materials [1]. It was designed to test TIMs at controlled bond line thickness (BLT) and controlled pressure, while being able to directly measure the bond line thickness. Solbrekken's tester can be used to measure the thermal impedance of a TIM with the minimum measurable limit of 0.03 K cm^2/W at a 95% confidence level. Zhang et al. developed a phase changeable material (PCM) with alkyl methyl silicone (AMS) waxes [2]. They also developed PCM composites composed of aluminum mesh and the AMS wax [3]. The thermal conductivity of PCM composites measured at temperatures above the phase change point of a wax is 7 W/mK, which is higher than that without the aluminum mesh, 4.3 W/mK. The PCM composites developed by Zhang et al. showed thermal impedance of 0.24 K cm^2/W at bond line thickness (BLT) of 115 μm. Instead of using a PCM, Lehmann and Davidson introduced a low melting temperature alloy (LMTA) whose melting point is 47°C with various fillers of conductive metals (44.7Bi, 22.6Pb, 19.1In, 8.3Sn, 5.3Cd) [4]. Webb et al. designed a new apparatus and a LMTA whose melting points are from 47.2°C to 81°C [5,6]. They reported that the thermal impedance of their LMTA is around 0.058 K cm^2/W. Most recently, they showed the thermal impedance of the LMTA-based TIM to be as low as 0.03 K cm^2/W [5–7].

The ASTM D5470 illustrates a standard method for measuring the thermal impedance of a TIM. A TIM is inserted between two metal bars whose top and/or bottom temperatures are measured by thermocouples. The thickness of the thermocouples used in the above experiment is 0.5–1.0 mm, which is thicker than the TIM, and each thermocouple measures only a spot temperature. The accuracy of the ASTM D5470 apparatus is not good. In this paper, we propose an apparatus for measuring thermal impedance and resistance using thermometer principles. This new apparatus consists of an alumina substrate, titanium tungsten (TiW) layers, gold layers, and thin alumina layers with a total thickness of about 5 microns, which is much thinner than the thermocouples.

In addition, we propose a new TIM that consists of carbon nanotubes and a thermally conductive matrix, and its thermal impedance is measured by the proposed new apparatus. The proposed TIM does not require any pad, a requirement for LMTAs, and therefore the thickness of our TIM is within 10 microns. A thermal resistor network model for the TIM is also developed here, and the predicted thermal properties of the TIM are compared with the experimental data.

2 Experimental Setup and Procedure

2.1 Design of a Thermal Property Measurement Apparatus. One-dimensional heat conduction under steady-state conditions is given by

$$\frac{Q}{A} = K\frac{\Delta T}{\Delta x} \tag{1}$$

where Q is the heat flow, (W), A, Δx, and K are surface area, thickness and the thermal conductivity of a specimen, respectively, and ΔT is temperature difference between high (T_h) and low (T_l), see Fig. 1(a).

Thermal resistance R (K/W) is defined from Eq. (1).

$$R = \frac{\Delta T}{Q} = \frac{T_h - T_l}{Q} = \frac{t}{KA} \tag{2}$$

Sometimes, thermal impedance θ (K cm^2/W) is a convenient property which is defined as

$$\theta = RA = \frac{t}{K} \tag{3}$$

Contributed by the Electronic and Photonic Packaging Division of ASME for publication in the JOURNAL OF ELECTRONIC PACKAGING. Manuscript received September 26, 2004; final manuscript received September 23, 2005. Review conducted by Koneru Ramakrishna.

 Copyright © 2006 by ASME

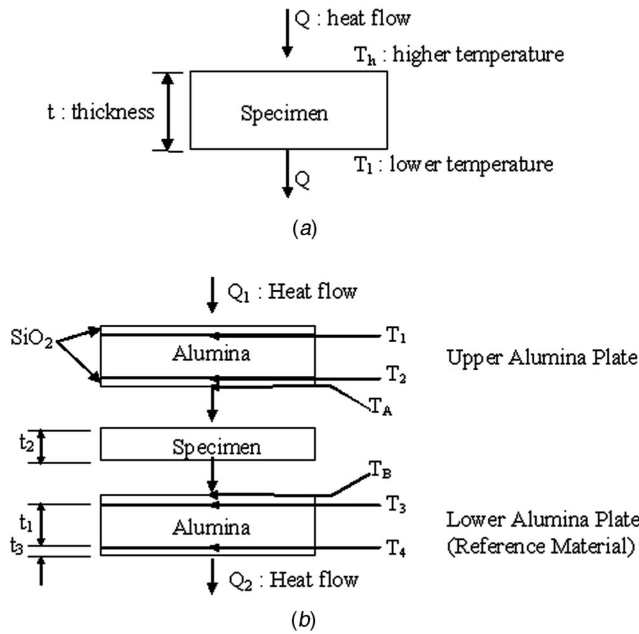

Fig. 1 Schematic diagrams: (*a*) 1D heat flow, and (*b*) two alumina substrates and specimen

Referring to Fig. 1(*a*) and the above thermal properties, we need to accurately measure heat flow Q and temperatures at the upper part (T_h) and lower part (T_l) of the specimen assuming one-dimensional heat flow downward.

In order to measure Q, T_h and T_l accurately, we designed an apparatus composed of upper and lower substrates, Fig. 1(*b*), where T_h and T_l are represented as T_A and T_B, respectively. The upper and lower substrates are made of alumina and a resistor circuit which functions as a thermometer, see Fig. 2.

When selecting a reference material, its thermal impedance should have a value similar to that of the TIM, 0.05–0.3 K cm^2/W. For alumina with a thermal conductivity of 25 W/mK and a thickness of 1.27 mm, its thermal impedance is 0.48 K cm^2/W by Eq. (2) [8]. Therefore, we choose an alumina substrate of this dimension for the reference material. The thermometer is a 35 mm × 30 mm rectangular shape, as shown in Fig. 2(*a*). 5 mm × 30 mm of the thermometer's area is connected to lead wires, as shown in Fig. 2(*b*). In order to construct a thermometer, three layers of metals (TiW+Au+TiW) are deposited on the surfaces of the alumina substrate. The temperature in the metal resistor layers is measured using the change in the electrical resistance of the layers.

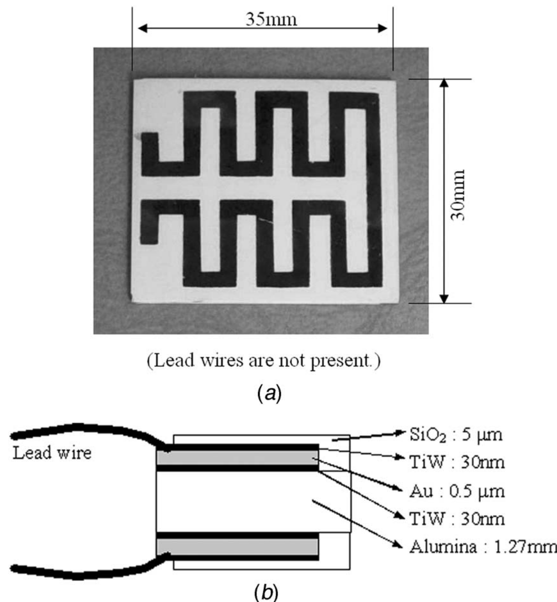

Fig. 2 A new apparatus: (*a*) photo of the alumina substrate, and (*b*) cross-sectional view of the alumina substrate

To construct the thermometer, TiW is first deposited on the alumina substrate by sputtering. This 30 nm TiW layer prevents gold (Au) particles from penetrating into the alumina substrate and enhances the bonding forces between the Au and alumina substrates. A 0.5 μm thick Au layer is deposited on the first TiW layer, and a second 30 nm thick TiW layer is deposited on top of the Au layer for better adhesion between the Au layer and a 5 μm SiO_2 layer, which is deposited uppermost. An additional 5 μm SiO_2 layer is deposited on the bottom surface. These SiO_2 layers act as an electrical insulator preventing direct contact between the metal layers and the specimen, i.e., the TIM.

In Fig. 1(*b*), T_A is the temperature on the bottom surface of the upper alumina substrate and T_B is the temperature on the top surface of the lower alumina substrate. t_1, t_2, and t_3 are the thickness of the alumina, the specimen, and the SiO_2 layer, respectively. For the upper alumina substrate, Q_{Alumina} and Q_{SiO_2} are calculated as

$$Q_{\text{Alumina}} = \frac{(T_1 - T_2) \times A}{\theta_{\text{Alumina}}} \tag{4}$$

$$Q_{\text{SiO}_2} = \frac{(T_2 - T_A) \times A}{\theta_{\text{SiO}_2}} \tag{5}$$

$$Q_{\text{Alumina}} = \frac{(T_3 - T_4) \times A}{\theta_{\text{Alumina}}} \tag{6}$$

With Eqs. (4)–(6) and assuming $Q_{\text{Alumina}} = Q_{\text{SiO}_2}$, T_A and T_B are expressed as

$$T_A = T_2 - \frac{\theta_{\text{SiO}_2}}{\theta_{\text{Alumina}}}(T_1 - T_2) \tag{7}$$

$$T_B = T_3 + \frac{\theta_{\text{SiO}_2}}{\theta_{\text{Alumina}}}(T_3 - T_4) \tag{8}$$

From Eq. (3), the thermal impedance θ is defined as thickness divided by thermal conductivity. The thermal conductivities of alumina and SiO_2 are reported as 25 W/mK and 1.5 W/mK, respectively [8], and the thickness of alumina and SiO_2 are measured as 1.27±0.02 mm and 5±0.1 μm, respectively. Therefore, the thermal impedance of alumina and SiO_2 are calculated as 0.48 K cm^2/W and 0.03 K cm^2/W, respectively.

According to the manufacture's data sheet, the thermal conductivity of alumina is around 28 W/mK at 20°C and 21 W/mK at 100°C. The temperature range of the alumina substrates is 45–55°C, so the thermal conductivity of the alumina substrates ranges from 24.8 to 25.4 W/mK. Because the thermal conductivity of alumina depends on temperature, an arbitrary constant value (25.0 W/mK) was chosen to calculate the thermal conductivity of the specimens. For SiO_2, thermal conductivity varies based on deposition conditions. The thickness of the SiO_2 layer is 5±0.1 μm. Because it is very difficult to measure the thermal conductivity of each SiO_2 layer, a constant value of 1.5 W/mK was arbitrarily chosen for calculations.

Based on Eqs. (7) and (8), and using the measured temperatures, T_1–T_4, one can calculate T_A and T_B which are set equal to

T_h and T_l, respectively. Therefore, thermal resistance R and thermal impedance θ of a specimen will be calculated by Eqs. (2) and (3), respectively.

2.2 Thermal Interface Material. A TIM usually consists of thermally conductive fillers and a matrix. Fillers transfer heat rapidly, while the matrix facilitates the installation of a TIM between the chip and a heat spreader or sink. The goal of developing new TIMs is to reduce thermal resistance (R) defined by Eq. (2), or, equivalently thermal impedance (θ) defined by Eq. (3). Since the surface area of a chip is predetermined, there exists only two parameters that we can modify to achieve lower values for R and θ, i.e., reduction of thickness (t) and increase in the thermal conductivity (K) of the TIM. The thermal conductivity K can be increased by increasing the volume fraction of the conductive fillers, but this would make the viscosity of the TIM higher, and make it more difficult for a packaging engineer to install the TIM. In addition to the volume fraction, filler size, filler shape, thermal conductivity of the fillers and matrix, and pressure applied during installation, manufacturing procedures can influence the thermal resistance and impedance of a TIM.

Filler, Matrix, and Solvent. In this study, carbon nanotubes and silicon thermal grease are chosen as filler and matrix, respectively. The carbon nanotubes are made by the CNI Company, in Houston, TX, and the silicon thermal grease is made by Epoxies Company, in Cranston, RI. A scanning electron microscopy (SEM) photo of the CNI carbon nanotubes is shown in Fig. 3(*a*). Chloroform was chosen as a solvent, because it dissolves the matrix material, thermal grease, and it is environmentally benign.

Two different compositions were prepared, as shown in Table 1. For composition 1, the carbon nanotubes and the silicon thermal grease were weighed and found to be 0.0508 g, and 0.1062 g, respectively. The carbon nanotubes, silicon thermal grease, and chloroform were inserted into a beaker together at room temperature and ultrasonic power was applied to spread the carbon nanotubes uniformly. After mixing, the chloroform was evaporated until only a small amount of chloroform remained in the TIM. Composition 1 had a total weight of 0.2231 g. The specific gravities of the carbon nanotubes, silicon thermal grease, and chloroform were 1.33, 2.30, and 1.48, respectively. Therefore, the volume fraction of the filler was 16.2%, that of the matrix was 19.6% and the balance was the solvent. This TIM was inserted into alumina substrates and spread over a 30 mm $\times$ 30 mm area. After evaporating the chloroform further, the microstructure of the TIM was captured by SEM, Fig. 3(*b*). Figure 3(*b*) shows that the carbon nanotubes are coated with silicon thermal grease.

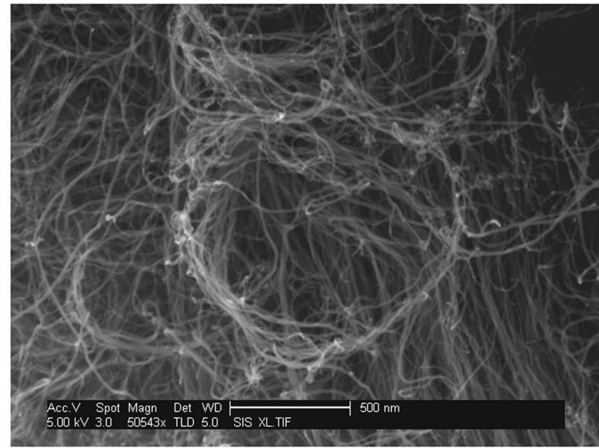

(*a*)

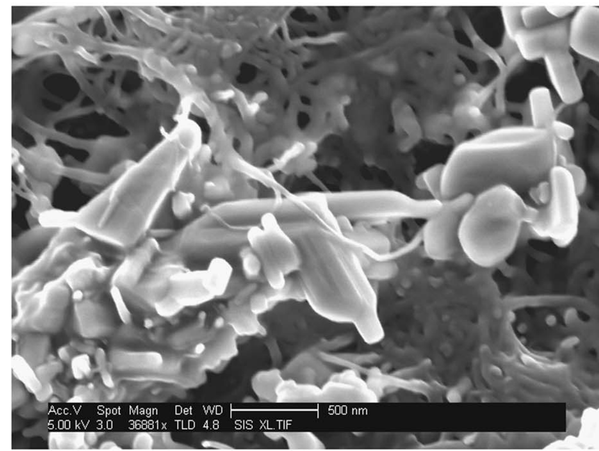

(*b*)

Fig. 3 Scanning electron microscopy (SEM) photos: (*a*) carbon nanotubes, (*b*) carbon nanotubes and matrix

3 Experimental Results

3.1 Thermal Impedance Measurements. Two alumina substrates with resistance thermometers made of Au-TiW layers (see Fig. 2) and a standard thermocouple were placed into a furnace with a known temperature. The electrical resistance of the thermometers was measured as a function of the furnace temperature. Figure 4 shows that the measured electrical resistance is a linear function of temperature. Figure 4 is used as a calibration data set by which the measured electric resistances are converted to temperatures.

The experimental setup of the thermal property measurement apparatus is shown in Fig. 5. In order to fix the thickness of a TIM specimen, 4 thin paper spacers of known thickness were placed between the two alumina substrates as shown in Fig. 5(*b*).

First, we measured the thermal properties of a commercial TIM made of PCM composite. Figure 6 shows the measured thermal impedance of the PCM composite vs spacer thickness which is specimen thickness, t. These tests were performed under a constant pressure of 3.0 ± 0.1 MPa at constant temperature of $50 \pm 2\,^{\circ}\mathrm{C}$. According to Fig. 6, the thermal impedance of the PCM increases linearly with thickness t, with a y-axis intercept of $0.081\ \mathrm{K\,cm^2/W}$. This y-axis intercept is defined as the thermal interface impedance (θ_{inter}). The intrinsic thermal impedance of a TIM, θ_{intrin}, which is obtained by subtracting θ_{inter} from total thermal impedance θ_{total}, is linearly proportional to specimen thickness t. The thermal interface impedance, θ_{inter}, is strongly influenced by the roughness of the upper and lower surfaces of the alumina substrates. In addition, thermal interface impedance, θ_{inter}, depends on material properties of the thermal interface material between these two surfaces. Therefore, thermal interface impedance measured by PCM composite is different from that measured by the carbon-nanotube-based TIM specimen we made. Because it is difficult to measure thermal interface impedance using the specimen, thermal interface impedance measured by the PCM composite is used to calculate intrinsic thermal impedance of the specimen. So, the intrinsic thermal impedance of the speci-

Table 1 Two different compositions of the composite specimen

	Filler (carbon nanotube)	Matrix (Silicon thermal grease)	Solvent (chloroform)
Composition 1	0.0508 g ($0.0382\ \mathrm{cm^2}$)	0.1062 g ($0.0462\ \mathrm{cm^2}$)	0.2231 g ($0.1507\ \mathrm{cm^2}$)
Composition 2	0.0232 g ($0.0174\ \mathrm{cm^2}$)	0.0958 g ($0.0417\ \mathrm{cm^2}$)	0.2012 g ($0.1359\ \mathrm{cm^2}$)

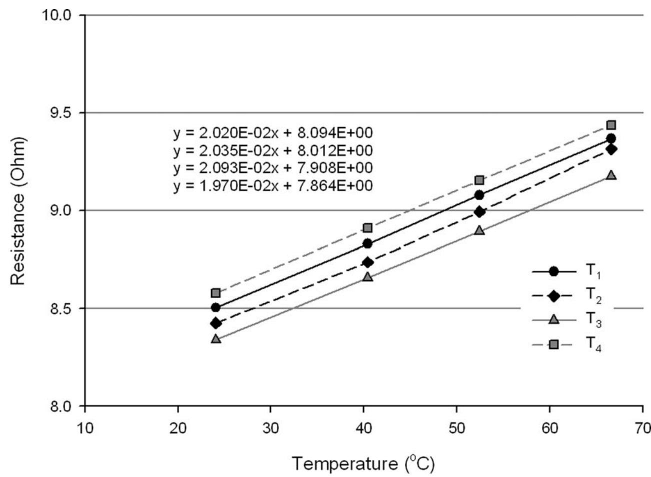

Fig. 4 Electrical resistance vs temperature

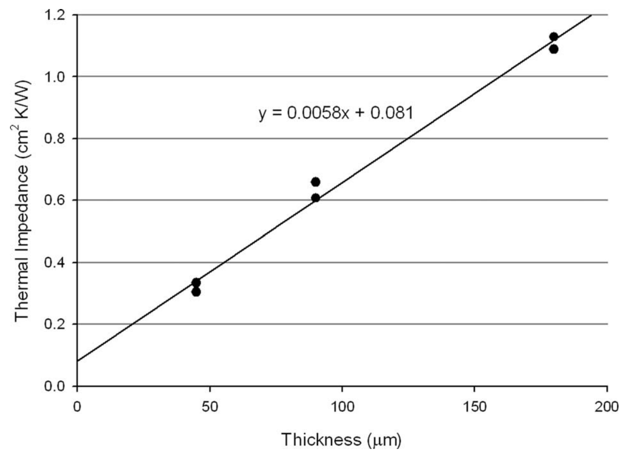

Fig. 6 Thermal interface impedance of the apparatus

men in the following calculation includes the difference between thermal interface impedance measured by PCM composite and actual thermal interface impedance using the specimen.

3.2 Thermal Impedance of Carbon-Nanotubes-Based TIM. The thermal impedance of the carbon-nanotube-based TIM specimen was measured under a constant applied stress of 3.0 ± 0.1 MPa and a constant temperature of $50\pm2°$C. The dimension of the TIM specimen was the same as before, i.e., 30 mm $\times$30 mm.

When steady-state heat conduction was reached, temperatures T_1, T_2, T_3, and T_4 were measured with the thermometer based on electrical resistance (Fig. 5). The temperatures at the top (T_A) and at the bottom (T_B) of the TIM specimen were calculated using Eqs. (7) and (8). For the TIM specimen of composition 1, five measurements were performed to obtain five thermal impedance values ranging from 0.0265 to 0.0399 K cm^2/W with an average value of 0.0321 K cm^2/W. By Eq. (2) and using a constant specimen thickness of 9.5 μm, the thermal impedance was converted to thermal conductivity. The values for thermal conductivity range from 2.38 to 3.58 W/mK, with an average value of 2.963 W/mK. For the TIM specimen of composition 2, thermal impedance was also measured five times, with values ranging from 0.0563 to 0.0772 K cm^2/W and an average value of 0.0654 K cm^2/W. By Eq. (2) and using a constant specimen thickness of 9.0 μm, the thermal impedance was converted to a thermal conductivity range of 1.166–1.600 W/mK, with the average being 1.376 W/mK.

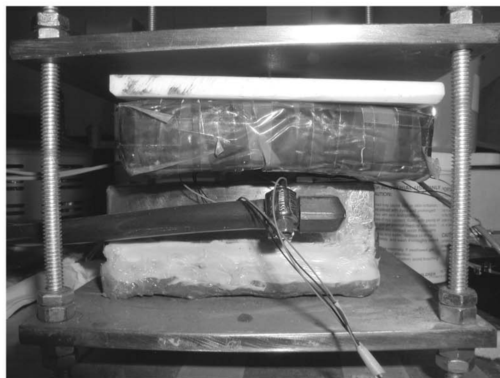

(*a*)

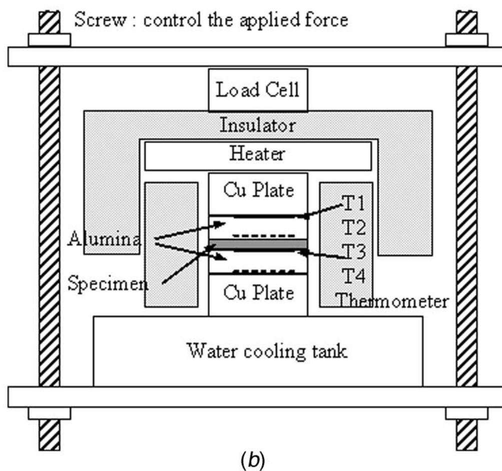

(*b*)

Fig. 5 Experimental setup: (*a*) photo of experimental setup, and (*b*) a schematic sketch

Uncertainty in the Data. It is important to note here that there are many factors which may have introduced uncertainties into the measured temperatures, T_1–T_4, and the heat flow, Q. Some of these are discussed below.

Measured Thickness of Specimens. According to Eqs. (2) and (3), the thermal conductivity of a specimen is calculated using the measured thermal impedance and the measured thickness. Each specimen is of a unique thickness. However, we did not find a method to measure specimen thickness during the experiment. Therefore, we measured a single specimen for each composition, and assumed all of the specimens of each composition to be of the same thickness in the calculations (9.5 μm for composition 1 and 9.0 μm for composition 2). Because the specimens are likely to differ in thickness, this may have introduced some degree of error.

The Thermal Conductivity of Alumina. The thermal conductivity of the upper alumina substrate should be lower than that of the lower alumina substrate. However, we assigned both substrates a common value (25.0 W/mK) to facilitate calculation. Because the thermal conductivity of the alumina substrates was calculated by linear interpolation, this value is approximate.

The Thermal Conductivity of SiO_2. The thermal conductivity of SiO_2 varies over deposition conditions. It is obvious that the thermal conductivity of the SiO_2 thin layers is different from that of SiO_2 bulk material. However, it is very difficult to take into consideration the diverse deposition conditions of all the SiO_2 thin films.

Parallel Surface. Although stress was applied uniformly, the upper and lower alumina substrates are not perfectly parallel. Therefore individual specimens may be of inconsistent thickness, resulting in further errors.

Misalignment of the 2 Alumina Substrates. The two alumina substrates may have become misaligned, leading to errors in the cross-sectional area.

Heat Loss. As shown in Fig. 5(*b*), insulation material was used to ensure 1D heat flow. Despite the use of insulation material, it is not possible to achieve perfect 1D heat flow, with no heat loss. However, we follow common practice and assume that the insulation provides 1D heat flow without lateral heat loss, and no factor is needed.

4 Comparison With Predictions by Resistor Network Model

In order to study the dependence of filler volume fraction on TIM conductivity, we attempted to predict the thermal conductivity of a TIM with carbon-nanotube fillers. There exist a number of models based on effective medium theory for predicting the thermal conductivity of a composite composed of conductive fillers and matrix. However, in these models, the shapes of the fillers are simple, short fillers, flakes and spherical particles, and they are assumed to be of the same size, whereas the microstructure of carbon-nanotubes is far more complex, as evidenced by Fig. 3(*a*). Therefore we employ a three-dimensional (3D) resistor network model which is explained below.

4.1 Resistor Network Model. The resistor network model is based on a three-dimensional (3D) cuboidal shape, Fig. 7(*a*), where the dark rectangular rods represent the conductor elements and the white areas represent the matrix. The top and bottom surfaces of the 3D cuboidal TIM specimen are assumed to be thermal conductors and all four side surfaces are adiabatic wall.

A unit cube consists of six identical resistors with half of the resistance of the site, as shown in Fig. 7(*b*). A thermal resistance of a resistor R_i can be obtained from the known thermal conductivity K_i of the *i*th unit cube using Eq. (2) as

$$R_i = \frac{\Delta x/2}{K_i \Delta x^2} = \frac{1}{2K_i \Delta x} \quad (9)$$

Thermal resistance R_{ij} between sites *i* and *j* is given, as shown in Fig. 7(*c*).

$$R_{ij} = R_i + R_j = \frac{1}{2\Delta x}\frac{K_i + K_j}{K_i K_j} \quad (10)$$

To facilitate the computation, thermal resistance is replaced by thermal conductance using its reciprocal relation. Thermal conductance G_{ij} between two sites (*i* and *j*) is defined by

$$G_{\mathrm{ij}} = \frac{1}{R_{\mathrm{ij}}} = \frac{2\Delta x \mathrm{K}_i K_j}{K_i + K_j} \quad (11)$$

A simplified computation flow chart of the resistor network model is shown in Fig. 8. First, the centroid fillers are seeded in a model cube by using a pseudo-random variable generator [9]. Then, fillers and clusters of filler are identified. Thermal conduction equations are established. According to the thermal conduction equations, the temperature at each site is solved with the known thermal conductance between sites by using Kirchhoff's equation and an iterative relaxation procedure. The details of the formulation of the 3D resistor network model are given in the Appendix. Finally, the thermal conductance and thermal conductivity of a composite are calculated by Eq. (12) and Eq. (13), respectively,

$$G_c = \frac{Q_c}{T_{\mathrm{Top}} - T_{\mathrm{Bottom}}} \quad (12)$$

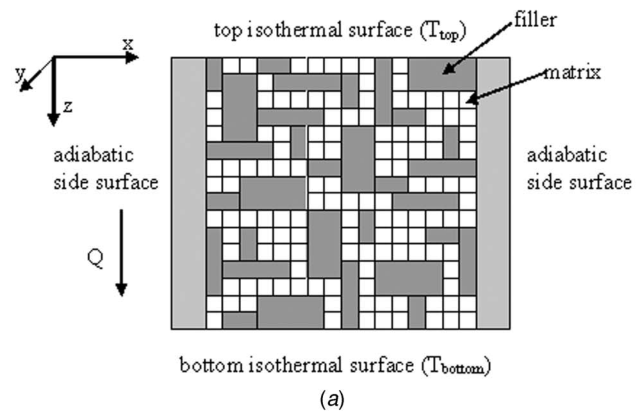

(*a*)

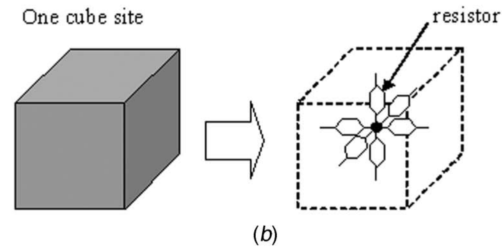

(*b*)

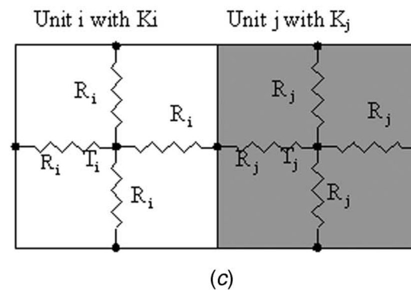

(*c*)

Fig. 7 Thermal resistor model: (*a*) thermal resistor network in a 3D simple cubic lattice system viewed by a 2D section, (*b*) resistors of unit cube, and (*c*) thermal resistance of two resistors

$$K_c = G_c \frac{L_z}{L_x L_y} \quad (13)$$

where L_z is the thickness of the composite specimen in the heat flow direction (*z*-axis), and the product of L_x and L_y is its cross-sectional area.

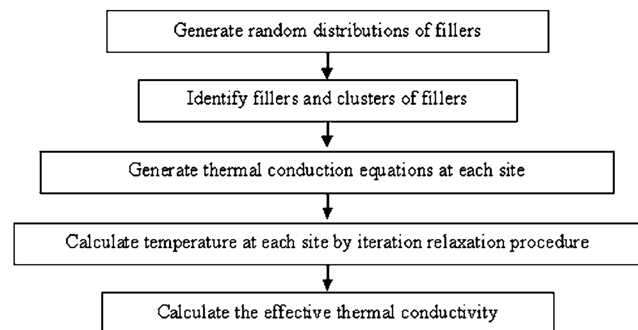

Fig. 8 Computation procedure of thermal resistor network model

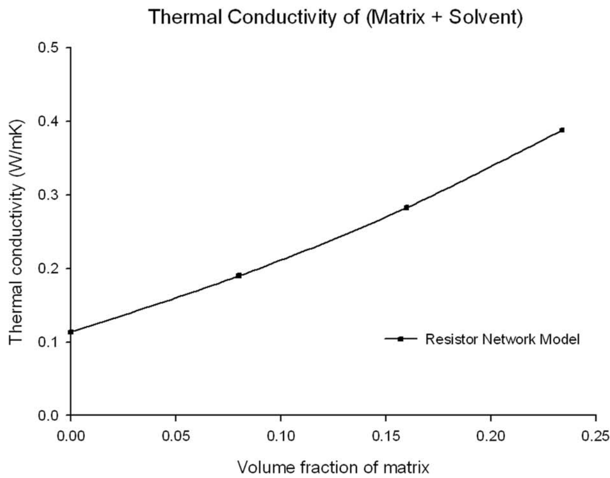

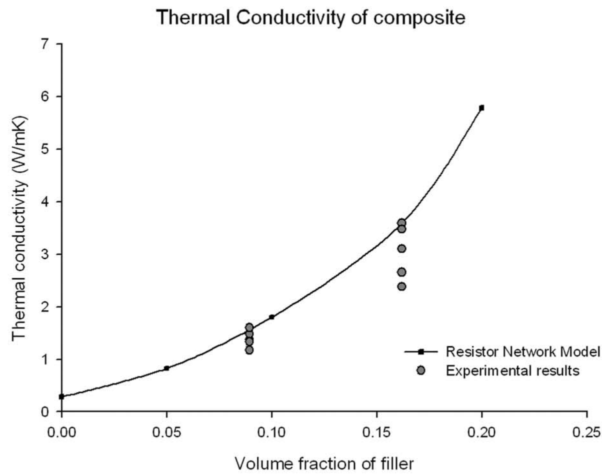

Fig. 9 Thermal conductivity calculated by resistor network model and measured by the apparatus; (*a*) step 1; thermal conductivity of matrix+solvent, and (*b*) step 2; thermal conductivity of the composite

4.2 Predictions by Resistor Network Model. The composite in the present study is composed of three different components; filler, matrix, and solvent. However, the present resistor network model assumes that a composite is composed of two components. So, for convenience we consider the matrix of silicon thermal grease and solvent to be a single component.

The thermal conductivity of silicon thermal grease is 1.2 W/mK and that of chloroform is 0.11 W/mK [10]. For both compositions (composition 1 and composition 2), the volume fraction of silicon thermal grease is 23.4%, while that of chloroform is 76.6%. The total size of the matrix is $3.0\times5.0\times5.0$ μm, and the dimensions of the silicon thermal grease are $0.5\times0.05\times0.05$ μm. During the iteration, a convergence error criterion of 1.0×10^{-5} is used for the successive temperature convergence. The predicted results of the thermal conductivity of the converted matrix material are shown in Fig. 9(*a*). When the volume fraction of silicon thermal grease is 23.4%, the thermal conductivity of the matrix is estimated by Fig. 9(*a*) as 0.3879 W/mK.

It is assumed that the thermal conductivity of the carbon nanotubes is 2000 W/mK [11], and that of the matrix is 0.3879 W/mK. The volume fractions of the carbon nanotubes are 16.2% for composition 1 and 8.9% for composition 2. The total dimensions of the TIM is $3.0\times5.0\times5.0$ μm, and the dimension of each filler is $0.5\times0.05\times0.05$ μm. Each filler is randomly placed into the matrix, but only 20% of fillers are oriented to the z-axis because the materials are spread into an x-y plane during the processing. The thermal conductivity of the TIM calculated by the 3D resistor network model is shown in Fig. 9(*b*). For the TIM of composition 1 with a 16.2% volume fraction of filler, the thermal conductivity of the composite is predicted to be 3.572 W/mK.

The experimental data of the thermal impedance of the TIMs (composition 1 and composition 2) are converted into thermal conductivity values using Eq. (2) and the results are shown in Fig. 9(*b*), where a composite thickness of 9.5 μm for composite 1 and 9.0 μm for composite 2 are used. The experimental data are close to the predictions by the 3D resistor network model.

5 Conclusion

A new apparatus with thermometers based on electric resistance is developed to measure the thermal impedance of TIMs. The thermal impedance of a TIM consists of thermal interface impedance (θ_{inter}) and thermal intrinsic impedance (θ_{intrin}). The θ_{inter} of the apparatus using PCM composite was found to be 0.081 K cm^2/W. A very thin TIM composed of carbon nanotubes, silicon thermal grease, and chloroform was developed. It has very low thermal impedance, i.e., $\theta_{\text{intrin}}=0.0265-0.0399$ K cm^2/W with an average value of 0.0321 K cm^2/W for composite 1. A 3D resistor network model was developed and compared with the experimental data. Simulation results using the resistor network model are in good agreement with the experimental data.

Nomenclature

A = cross-sectional area (m^2)
G = thermal conductance (W/K)
K = thermal conductivity (W/mK)
L = length (m)
Q = heat flow (W)
R = thermal resistance (K/W)
t = thickness (m)
T_h = higher temperature (K)
T_l = lower temperature (K)

Greek

θ = thermal impedance (K m^2/W or K cm^2/W)
ρ = thermal resistivity (mK/W)

Appendix: Formulation of 3D Resistor Network Model

The temperature at each site is solved with the known thermal conductance between sites using Kirchhoff's equation and an iterative relaxation procedure.

$$Q_i = \sum_j G_{ij}(T_i - T_j) \tag{A1}$$

Equation (A1) illustrates heat flow Q_i going into and out of site i from the nearest neighboring sites. T_i is the temperature at site i, G_{ij} is the thermal conductance between sites i and j, and T_j are the temperatures of neighbor sites. Following the first law of thermodynamics (the principle of energy conservation), analogous to the Kirchhoff's current law, the net heat flow Q_i is zero except for the external terminals, because there is no heat source in site i. The first law of thermodynamics is expressed as Eq. (A2).

$$Q_i(i-1,j,k) + Q_i(i+1,j,k) + Q_i(i,j-1,k) + Q_i(i,j+1,k) + Q_i(i,j,k-1) + Q_i(i,j,k+1) = 0 \tag{A2}$$

A substitution of Eq. (A1) into (A2) gives Eq. (A3).

$$G\left(i-\tfrac{1}{2},j,k\right)\{T(i,j,k)-T(i-1,j,k)\}+G\left(i+\tfrac{1}{2},j,k\right)\{T(i,j,k)-T(i+1,j,k)\}+G\left(i,j-\tfrac{1}{2},k\right)\{T(i,j,k)-T(i,j-1,k)\}+G\left(i,j+\tfrac{1}{2},k\right)\{T(i,j,k)-T(i,j+1,k)\}+G\left(i,j,k-\tfrac{1}{2}\right)\times\{T(i,j,k)-T(i,j,k-1)\}+G\left(i,j,k+\tfrac{1}{2}\right)\{T(i,j,k)-T(i,j,k+1)\}=0 \quad \text{(A3)}$$

Equation (A3) is rewritten as Eq. (A4),

$$T(i,j,k)=CM1(i,j,k)T(i-1,j,k)+CM2(i,j,k)T(i+1,j,k)+CM3(i,j,k)T(i,j-1,k)+CM4(i,j,k)T(i,j+1,k)+CM5(i,j,k)T(i,j,k-1)+CM6(i,j,k)T(i,j,k+1) \quad \text{(A4)}$$

where

$$CM(i,j,k)=G\left(i-\tfrac{1}{2},j,k\right)+G\left(i+\tfrac{1}{2},j,k\right)+G\left(i,j-\tfrac{1}{2},k\right)+G\left(i,j+\tfrac{1}{2},k\right)+G\left(i,j,k-\tfrac{1}{2}\right)+G\left(i,j,k+\tfrac{1}{2}\right)$$

$$CM1(i,j,k)=G\left(i-\tfrac{1}{2},j,k\right)/CM(i,j,k)$$

$$CM2(i,j,k)=G\left(i+\tfrac{1}{2},j,k\right)/CM(i,j,k)$$

$$CM3(i,j,k)=G\left(i,j-\tfrac{1}{2},k\right)/CM(i,j,k)$$

$$CM4(i,j,k)=G\left(i,j+\tfrac{1}{2},k\right)/CM(i,j,k)$$

$$CM5(i,j,k)=G\left(i,j,k-\tfrac{1}{2}\right)/CM(i,j,k)$$

$$CM6(i,j,k)=G\left(i,j,k+\tfrac{1}{2}\right)/CM(i,j,k) \quad \text{(A5)}$$

The adiabatic boundary condition is applied to the side surfaces and the isothermal boundary condition is applied to the top and bottom surfaces. Theses boundary conditions are expressed as Eqs. (A6) and (A7).

Adiabatic B.C.

$$T(1,j,k)-T(2,j,k)=0$$

$$T(x\,\max-1,j,k)-T(x\,\max,j,k)=0$$

$$T(i,1,k)-T(i,2,k)=0$$

$$T(i,y\,\max-1,k)-T(i,y\,\max,k)=0 \quad \text{(A6)}$$

Isothermal B.C.

$$T(i,j,1)=T_{\text{Top}}=1$$

$$T(i,j,k)=T_{\text{Bottom}}=0 \quad \text{(A7)}$$

With the adiabatic and isothermal boundary conditions and the iteration method, Eq. (A4) is rewritten as Eq. (A8)

$$T^{(n+1)}(i,j,k)=CM1(i,j,k)T^{(n+1)}(i-1,j,k)+CM2(i,j,k)\times T^{(n)}(i+1,j,k)+CM3(i,j,k)T^{(n+1)}(i,j-1,k)+CM4(i,j,k)T^{(n)}(i,j+1,k)+CM5(i,j,k)T^{(n+1)}\times(i,j,k-1)+CM6(i,j,k)T^{(n)}(i,j,k+1) \quad \text{(A8)}$$

where (n) is the iteration trial number.

After convergence of all temperature values is reached, the heat flow Q_c through the composite in the z-axis is calculated as Eq. (A9).

$$Q_c=\sum_{i,j}Q(i,j,z\,\max-1)=\sum_{i,j}G\left(i,j,z\,\max-\tfrac{1}{2}\right)\{T(i,j,z\,\max-1)-T(i,j,z\,\max)\}=\sum_{i,j}G\left(i,j,z\,\max-\tfrac{1}{2}\right)\{T(i,j,z\,\max-1)-T_{\text{Bottom}}\} \quad \text{(A9)}$$

Finally, thermal conductance and thermal conductivity of a composite are calculated by Eqs. (12) and (13), respectively,

$$G_c=\frac{Q_c}{T_{\text{Top}}-T_{\text{Bottom}}}$$

References

[1] Solbrekken, G., Chu, C., Byers, B., and Reichenbacher, D. 2000, "The Development of a Tool to Predict Package Level Thermal Interface Material Performance," 2000 Int. Society Conference on Thermal Phenomena, Las Vegas, NV, USA, 23–26 May, 2000 Vol. 1, pp. 48–54.

[2] Zhang, S., Swarthout, D., Feng, Q., Petroff, L., and Noll, T., "Alkyl Methy Silicone Phase Change Materials for Thermal Interface Applications," ITherm 2002 Proc., pp. 485–488.

[3] Zhang, S., "Silicone Phase Change Thermal Interface Materials: Property and Application," in Proc. of InterPACK 2003, Paper No. IPACK2003-35075.

[4] Lehaman, G., and Davidson, D., "Thermal Performance of Liquid Solder Joint Between Metal Faces," in Proc. of InterPACK 2001, Paper No. IPACK2001-15890.

[5] Gwinn, J., Saini, M., and Webb, R., "Apparatus for Accurate Measurement of Interface Resistance of High Performance Thermal Interface Materials," ITherm 2002 Proc., pp. 644–650.

[6] Webb, R., and Gwinn, J., "Low Melting Point Thermal Interface Material," ITherm 2002 Proc., pp. 671–676.

[7] Webb, R., and Paek, J., "Low Melting Point Alloy Thermal Interface Material: Further Results," Proc. of InterPACK 2003, Paper No. IPACK2003-35253.

[8] Hannemann, R., Kraus, A., and Pecht, M., 1994, *Physical Architecture of VLSI Systems*, Wiley, New York.

[9] Taya, M., and Ueda, N., 1987, "Prediction of the In-Plane Electrical Conductivity of a Misoriented Short Fiber Composite: Fiber Percolation Model Versus Effective Medium Theory," ASME J. Eng. Mater. Technol., **109**, pp. 252–256.

[10] http://www.cheric.org/kdb/kdb/hcprop/showcoef.php?cmpid=1518&prop=THG.

[11] Hone, J., 2001, "Phonons and Thermal Properties of Carbon Nanotubes," Carbon Nanotube Topics in Applied Physics, pp. 273–286.